Laser-induced structures in a polymer blend in the vicinity of the phase boundary

A. Voit, A. Krekhov, and W. Köhler*
Physikalisches Institut, Universität Bayreuth, D-95440 Bayreuth, Germany
(Received 8 March 2007; published 26 July 2007)

We have determined the diffusion, thermal diffusion, and Soret coefficients of a poly(dimethyl siloxane)/poly(ethyl-methyl siloxane) (PDMS/PEMS) polymer blend as a function of composition and temperature within the homogeneous phase. The critical slowing down of the diffusion and the corresponding critical divergence of the Soret coefficient are described within the pseudospinodal concept both for critical and off-critical compositions. These data are used to model in detail the channel-like structures that form due to the Soret effect when a focused laser beam is scanned across a polymer film of 100 μm thickness. A moderate vertical asymmetry is attributed to solutal convection. Although heat rapidly diffuses away from the laser focus, the composition distribution in the early stage resembles the sharp profile of the laser beam. PDMS accumulates within the center of the structures, whereas a thin PEMS-rich layer is formed that isolates the central core from the windows. Experimentally, the structures are analyzed by means of phase contrast microscopy. Possible applications as rewritable optical waveguides or tunable phase plates are briefly discussed.

DOI: 10.1103/PhysRevE.76.011808 PACS number(s): 61.25.Hq, 66.10.Cb

I. INTRODUCTION

Much work has been devoted to the development of techniques for the structuring of thin polymer films. Most prominent examples are photoresists that undergo a crosslinking reaction upon irradiation with visible or ultraviolet light, x ray, or electron beams. Direct electron beam writing can be employed for the fabrication of optical waveguides [1]. Böltau *et al.* [2] have demonstrated that an incompatible polymer blend can translate the two-dimensional surface energy structure of a prepatterned substrate into a composition pattern, if the characteristic wavelength of the prepatterning is compatible with the intrinsic length scale of the free spinodal demixing morphology. A variation of the morphology of thin PMMA/SAN films has been achieved by Chung *et al.* by changing the PMMA content [3]. Naturally, such an approach is not suitable for the formation of, e.g., a single linear structure within an otherwise homogeneous film. Fytas and co-workers have observed pattern formation in homogeneous polymer solutions after laser irradiation [4,5], but the underlying mechanism is not yet understood.

In a previous work we have demonstrated that local heating of a polymer blend close to its critical point by a focused laser beam creates localized pointlike perturbations of the composition both in the homogeneous and in the demixed phase [6]. These local composition shifts are caused by the Soret effect, which accounts for a concentration gradient that develops in a multicomponent mixture subjected to an inhomogeneous temperature field. The Soret coefficient S_T, which is a measure for the stationary concentration change produced by a given temperature difference, can be very large near the critical temperature T_c of spinodal decomposition and diverges like $(T-T_c)^{-0.67}$ in the asymptotic critical and like $(T-T_c)^{-1}$ in the classical mean field regime [7,8]. Duhr and Braun have used this effect to write patterns into aqueous solutions of fluorescently tagged DNA [9].

In the present work we show that this mechanism can be utilized to create almost arbitrary two-dimensional structures in a thin polymer layer. We are not aware of any other existing technique that would allow for the reversible formation of such patterns, which are characterized by a continuous variation of the local polymer composition. Writing is easily accomplished by scanning the laser by means of a simple galvano scanner. The excursions along the composition axis can be significant and have reached up to 20% in either direction in our experiments. This can lead to rather complex scenarios where equilibrium phase diagrams no longer yield an adequate description. As an example, even UCST systems may be quenched into phase separation by local heating [10].

The channel-like structures written by the focused laser are transient, however, with a rather long lifetime of typically 10^3 s. Though the PDMS/PEMS system is not suitable for waveguide applications, since the channels have a lower instead of a higher refractive index than the surrounding material, such structures might be useful as erasable and dynamically reconfigurable waveguides. There is no physical reason that would prevent, in another system, the higher refractive index material from migrating towards the hotter central regions. Interestingly, a cladding layer that shields the channel from the substrate is automatically formed. By variation of the writing speed and/or the laser intensity, continuous variations of the contrast can easily be achieved. Another type of reconfigurable liquid waveguides, which are based on microfluidic technology, has recently been proposed by Wolfe *et al.* [11]. We have undertaken a substantial modeling effort in order to obtain a quantitative description of the three-dimensional temperature and composition field within the polymer layer. Since the transport coefficients strongly vary in the vicinity of the critical point, a realistic parametrization of all material parameters, especially of the diffusion and thermal diffusion coefficients as a function of both composition and temperature, was required. Consequently, the first part of the paper is about the measurement of these transport coefficients within the entire one-phase regime. These data provide the input for the fit of a two-dimensional model based on the so-called pseudospinodal concept. Fi-

*werner.koehler@uni-bayreuth.de

TABLE I. Properties of pure components. M molar mass, N degree of polymerization, polydispersity M_w/M_n, and n refractive index.

	M (kg/mol)	N	M_w/M_n	n
PDMS	16.4	219	1.10	$1.4116-3.7\times10^{-04}(T/K-273)$
PEMS	48.1	545	1.19	$1.4347-3.3\times10^{-04}(T/K-273)$

nally, this parametrization serves as a basis for the numerical simulations of the patterning experiments presented in this paper. We have also included solutal convection [12] which turns out to be the relevant mechanism for a slight vertical asymmetry. As far as we know, thermal diffusion and Soret coefficients are not known for any other polymer blend. We have chosen the PDMS/PEMS system for these first experiments since it is rather well characterized in terms of phase behavior [13], diagonal transport coefficients [13,14] and, at least for the critical composition, off-diagonal transport coefficients [7,15].

II. MEASUREMENT OF TRANSPORT COEFFICIENTS

A. Experiment

The system under investigation was PDMS (M_w =16.4 kg/mol) and PEMS (M_w=48.1 kg/mol). The degree of polymerization, polydispersity, and refractive index of the pure components is listed in Table I. Mixtures with different mass fractions c of PDMS were prepared. A negligible amount of an inert dye (quinizarin) was added which absorbs at the laser wavelength and allows for optical heating. The amount of dye has been chosen to result in an optical absorption coefficient of α=5 cm^{-1}. The samples were stirred and kept at temperatures high enough to ensure a perfect mixing of the two components. The homogeneous mixture was then filled in a quartz glass cuvette with a path length of 200 μm. The measurements of the transport coefficients were performed by a transient holographic grating technique described in detail elsewhere [16]. The typical fringe spacing of the transient grating was about 4 μm for off-critical, and 2 μm for critical compositions. The contrast factors of the investigated samples, obtained with an Abbe refractometer, are given in Table II. The cloud points (Fig. 4 below) of the samples were determined by a turbidity experiment.

B. Results

In a previous work [7] we have investigated diffusion and thermal diffusion of a critical PDMS/PEMS blend with molar masses of the two constituents of 16.4 kg/mol and 22.8 kg/mol, respectively. The critical temperature of this system was T_c=311.75 K and its critical composition c_c =0.548. For the laser-patterning experiments discussed later in this publication the molar masses (16.4 kg/mol and 15.9 kg/mol) and the locus of the critical point (T_c =290.15 K, c_c=0.48) are comparable and the convenient T_c allows experiments close to room temperature. For the determination of the transport coefficients within the entire one-phase region we were facing two problems. Firstly, the amount of material needed to perform concentration dependent measurements exceeded the available amount of PEMS (15.9 kg/mol), and a new synthesis of exactly the same molar mass is virtually impossible. Secondly, the accessible temperature range with our thermostated sample cell is limited to 0 °C$<T<$100 °C, which prohibits the measurement of significantly off-critical compositions down to the binodal if the critical temperature of an UCST system is already close to room temperature. In order to shift T_c towards the upper limit of the accessible temperature window, we employed a PDMS(16.4 kg/mol)/PEMS(48.1 kg/mol) blend with a critical temperature of $T_c \approx 354$ K and a critical composition of $c_c \approx 0.6$. Below, we will show how the data obtained for this system can be used for a reasonable parametrization of the transport coefficients in the laser-patterning experiment.

TABLE II. Fit results for T_{sp} and D_T^0 and contrast factors for the PDMS(16.4 kg/mol)/PEMS(48.1 kg/mol) blend.

c(PDMS) (g/g)	T_{sp} (K)	D_T^0 (10^{-7} cm^2 K^{-1}s^{-1})	$(\partial n/\partial T)$ (10^{-4} K^{-1})	$(\partial n/\partial c)$ (10^{-2})
0.090	230.0	1.62	−3.4	−2.4
0.197	265.6	1.50	−3.3	−2.4
0.300	313.4	1.70	−3.7	−2.4
0.399	334.8	1.65	−3.6	−2.4
0.499	350.2	1.32	−3.5	−2.4
0.609	352.6	3.07	−3.7	−2.4
0.690	353.5	1.87	−3.7	−2.4
0.790	316.5	1.91	−3.8	−2.4
0.900	244.8	2.35	−3.8	−2.4

Figure 1 shows the Soret and the diffusion coefficient of various PDMS/PEMS blends of critical or almost critical compositions as a function of the distance to the spinodal temperature $\epsilon=(T-T_{sp})/T$. On this reduced temperature scale the data points of all mixtures show a very similar temperature dependence, and even their absolute values coincide at least within a factor of two. This behavior is already a strong indication that the Soret, thermal diffusion, and diffusion coefficients of a blend with a particular PEMS molar mass can be estimated from the respective values obtained for a different molar mass by shifting the temperature scales such that the critical temperatures match. The dashed lines in the plot of S_T in Fig. 1 correspond to scaling laws of $S_T \propto \epsilon^{-1}$ within the classical mean field regime and $S_T \propto \epsilon^{-0.67}$ within the asymptotic critical region [7].

The diffusion and thermal diffusion coefficients measured for the PDMS(16.4 kg/mol)/PEMS(48.1 kg/mol) blend in the entire one-phase regime above the binodal are plotted in Fig. 2 and the Soret coefficients in Fig. 3. The critical composition of this system ($c_c \approx 0.6$) and the critical temperature ($T_c \approx 354$ K) are inferred from the cloud point curve as obtained from turbidity measurements.

The diffusion coefficient D shows the characteristic critical slowing down for concentrations close to c_c, whereas D_T

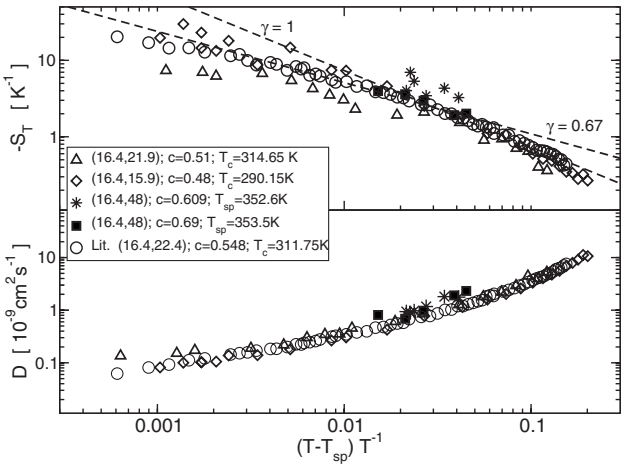

FIG. 1. Diffusion and Soret coefficient for critical and almost critical blends of PDMS(16.4 kg/mol) with varying molar mass of PEMS. The legends give the molar masses of PDMS and PEMS, the concentrations c and the critical temperature T_c. T_{sp} is the temperature of the spinodal (see text). Literature data (open circles) are taken from Ref. [7]. The dashed lines show the scaling behavior of $S_T \propto \epsilon^{-\gamma}$ with $\gamma=1$ for the mean field regime and $\gamma=0.67$ for the Ising regime.

does not show critical behavior and varies, for a given composition, only by thermal activation [7]. The concentration dependence of D_T is only weak. As a consequence, the temperature dependence of $S_T=D_T/D$ is moderate for off-critical compositions and pronounced close to c_c. $|S_T|$ reaches values of almost 10 K^{-1} for the near critical composition $c=0.609$ and the total experimentally observed variation of S_T covers almost two orders of magnitude. Directly at the critical point a critical divergence is expected, which can, of course, never be observed experimentally due to finite temperature modulation amplitudes in the holographic grating experiment and due to finite size effects [17].

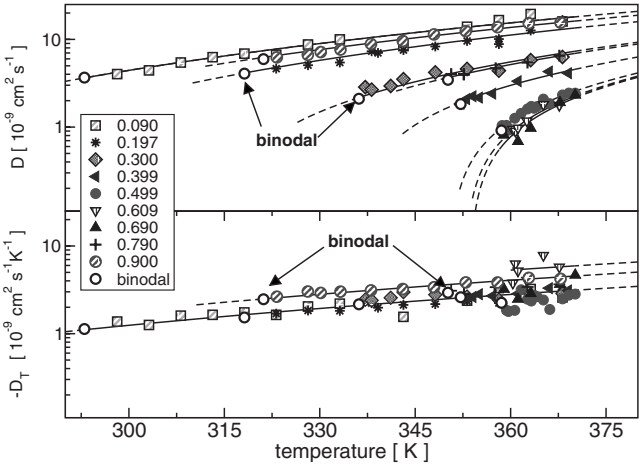

FIG. 2. Diffusion coefficient D and thermal diffusion coefficient D_T of PDMS(16.4 kg/mol)/PEMS(48.1 kg/mol) for different mass fractions of PDMS as indicated in the legend. For concentrations close to the critical concentration diffusion slows down approaching the phase boundary. The solid lines are fits of Eq. (1) for D_T and Eq. (4) for D. The dashed lines show an extension of the fitted function into the experimentally inaccessible range.

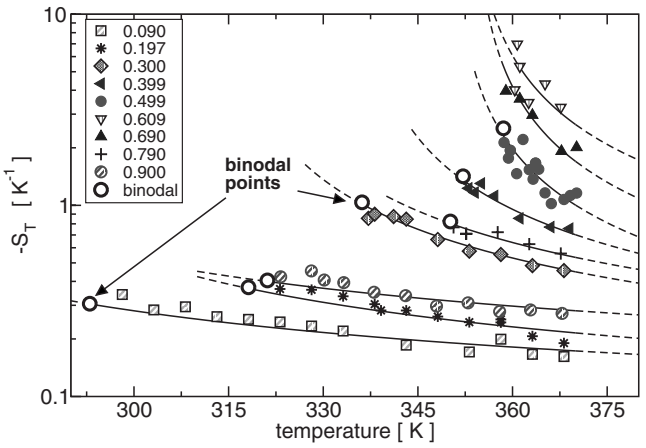

FIG. 3. Soret coefficients for different concentrations of PDMS(16.4 kg/mol)/PEMS(48.1 kg/mol). The solid lines are plots of $S_T=D_T/D$ with D_T and D according to Eqs. (1) and (4), respectively. D_T^0 and T_{sp} from Table II.

The interpolating curves in Figs. 2 and 3 are terminated at their low-temperature end by their intersection with the binodal line, which defines the phase boundary. These binodal points are marked with open circles. Below the binodal follows, except for the critical composition, the metastable regime, where measurements on a short time scale should still be possible. In practice, however, experiments are hampered by increasing background scattering due to nucleation and growth processes and we have restricted our experiments to the stable one-phase regime.

C. Parametrization of the transport coefficients

For the modeling of the laser-patterning experiments a parametrization of the transport coefficients within the one-phase regime is needed. In principle, this could be achieved by fitting suitable functions of the variables c and T with a sufficient number of free parameters to the measurements of Figs. 2 and 3. In order to derive simple model functions, which are based on a meaningful physical picture, we resort to the so-called pseudospinodal concept [18,19]. Within this framework, power laws with the same exponents as for the critical composition are assumed to hold also for off-critical samples. The divergence of the susceptibility and the vanishing of the diffusion coefficient do not occur at the critical temperature T_c but rather at the spinodal temperature T_{sp}, which is, for an UCST system, below the temperature of the binodal.

1. Thermal diffusion coefficient

The lower part of Fig. 2 shows the thermal diffusion coefficient D_T as a function of temperature within the homogeneous phase above the binodal. There is no sign of critical slowing down of D_T, and its temperature dependence follows thermal activation [7,8] as follows:

$$D_T = D_T^0 \exp(-T_A/T). \quad (1)$$

The activation temperature $T_A = 1460$ K has been determined in Ref. [7] for a PDMS(16.4 kg/mol)/PEMS(22.8 kg/mol) blend. With the same activation temperature, Eq. (1) also yields a good description for the PDMS(16.4 kg/mol)/PEMS(48.1 kg/mol) blend in Fig. 2. A fit of Eq. (1) to the measured data with a common T_A as adjustable parameter yields an almost identical value of $T_A = 1395$ K. The D_T^0 values hardly change over the entire composition range (Table II). This observation is a strong indication that the local friction experienced by the polymer segments, which strongly influences D_T in polymer solutions [20,21], remains almost constant. D_T^0 appears to be somewhat higher for the almost critical concentration $c = 0.609$, but, because of the high $T_c \approx 354$ K, only a very limited temperature range could be measured for this composition, and the critical slowing down of mass diffusion unavoidably increases the experimental error of D_T. We take an average value for D_T^0 from Table (2), which finally yields a parametrization of

$$D_T = [-1.88 \times 10^{-7} \text{ cm}^2(\text{s K})^{-1}]\exp(-1460 \text{ K}/T). \quad (2)$$

2. Diffusion coefficient

The diffusion coefficient of a critical mixture has been discussed in the comprehensive review of Luettmer-Strathmann [8] as follows:

$$D = \frac{\alpha^b + \Delta\alpha}{S(0)}. \quad (3)$$

α^b and $\Delta\alpha$ are the background contribution and the critical enhancement of the Onsager coefficient, respectively [22]. Since most measurements have been carried out at least a few K above the spinodal, we neglect $\Delta\alpha$ and assume thermal activation for α_b with the same activation temperature of $T_A = 1460$ K as for D [7]. The classical mean-field scaling exponent of the structure factor $S(0) \propto \epsilon^{-\gamma}$ is $\gamma = 1$, where $\epsilon = (T - T_c)/T$ is the reduced distance to the critical temperature. Occasionally, $(T - T_c)/T_c$ is used in the literature to measure the distance to the critical temperature. For small ϵ the difference is hardly noticeable and vanishes close to T_c. Because of the following arguments, we prefer ϵ as defined above.

Within the pseudospinodal concept it is assumed that the diffusion coefficient of an off-critical mixture can still be described according to Eq. (3), provided that the critical temperature T_c is replaced by the temperature of the spinodal T_{sp} at the respective concentration. Combining above arguments we end up with a temperature dependence of the diffusion coefficient of

$$D = a_0 \frac{T - T_{sp}}{T} \exp(-T_A/T). \quad (4)$$

The proportionality constant can be determined from the diffusion coefficients measured for the critical PDMS(16.4 kg/mol)/PEMS(22.8 kg/mol) mixture of Ref. [7] with $T_A = 1460$ K to $a_0 = 24.7 \times 10^{-7}$ cm^2 s^{-1}. T_{sp} is the only free parameter and is obtained from a fit of Eq. (4) to the measured $D(T)$ for every individual concentration c. The solid lines in the upper part of Fig. 2 show these fits, which, obviously, give an excellent parametrization of the measured data within the one-phase regime. The adjusted parameters T_{sp} are summarized in Table II for all concentrations.

Employing this a_0 value as a crude approximation also for off-critical compositions and for a different molar mass requires some justification. Below, we will present a simple physical picture that gives some insight into the structure of Eq. (4). In order to keep it simple, only symmetric mixtures are considered and a composition dependence of local friction, which could be dramatic for mixtures with one component close to its glass transition temperature [23], is not taken into account. Based on Eq. (4), an excellent parametrization of the experimental data is obtained as input for the numerical simulations. Because of the simplified physical model, the calculated spinodal line should, however, not be taken too literally.

Meier *et al.* [13,24,25] have investigated interdiffusion in a PDMS/PEMS blend. These authors start from the expression

$$D = \frac{\alpha^b}{S(0)} = \frac{\phi(1-\phi)W_0}{S(0)} \quad (5)$$

for the classical mean-field part of Eq. (3). Here, ϕ is the volume fraction of component A and $(1-\phi)$ the one of component B. W_0 is a local diffusion coefficient related to a Rouse diffusion coefficient D_R^0 by $W_0 = ND_R^0$ for unentangled chains of N segments.

Within the Flory-Huggins model the static structure factor of a critical system is expressed by the interaction parameter χ at the respective temperature and its value χ_c at the critical point [26],

$$S(0) = \frac{1}{2\chi_c}(1 - \chi/\chi_c)^{-1}. \quad (6)$$

The pseudospinodal concept is introduced by replacing χ_c for off-critical concentrations by the interaction parameter at the spinodal, χ_{sp} as follows:

$$D = \phi(1-\phi)W_0 2\chi_{sp}(1 - \chi/\chi_{sp}). \quad (7)$$

We can get rid of the factor $\phi(1-\phi)$ by remembering that for symmetric mixtures of equal degrees of polymerization N, the spinodal is given by [27]

$$\chi_{sp} = \frac{1}{2N\phi(1-\phi)}. \quad (8)$$

With the assumption of a purely enthalpic interaction parameter $\chi = a/T$ the diffusion coefficient finally becomes

$$D = \frac{W_0}{N}\frac{T - T_{sp}}{T}. \quad (9)$$

Equation (9) is equivalent to Eq. (4) with a thermally activated $W_0/N = a_0 \exp(-T_A/T)$.

Meier *et al.* have measured the concentration dependence of W_0 for a PDMS/PEMS blend for different temperatures

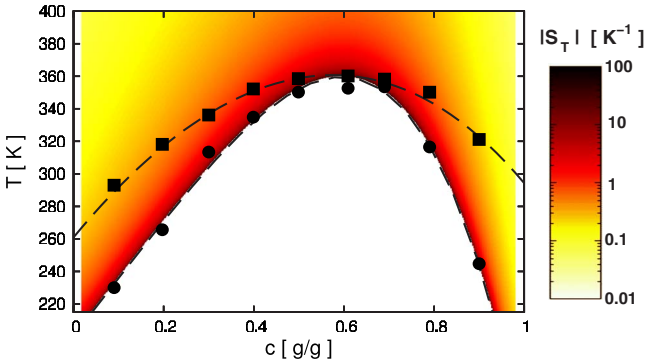

FIG. 4. (Color online) Phase diagram of polymer blend PDMS(16.4 kg/mol)/PEMS(48.1 kg/mol). The cloud points (filled squares) are obtained from turbidity measurements. The pseudospinodal points (filled circles) are only approximate and result from a fit of Eq. (4). The polynomial, describing T_{sp}, shown in the plot is used for parametrization. The color coding gives the absolute value of S_T in the one-phase region.

and found only a moderate concentration dependence of approximately a factor of 2 [24]. Somewhat more complicated expressions are obtained for asymmetric blends, but the general structure remains unchanged. The N^{-1} dependence in Eq. (9) introduces a molar mass dependence. Again, we expect the correction to be of the order of a factor of 2, since only the molar mass of the PEMS changes noticeably between the different samples discussed in this contribution. Another source of error comes from the neglect of the entropic part of the interaction parameter χ.

Nevertheless, since we do not intend to determine the true spinodal, Eq. (4) provides a simple two-dimensional model function for $D(c,T)$, which is based on a reasonable physical picture. There is only a single free fit parameter $T_{sp}(c)$ for every concentration c.

3. Soret coefficient

The Soret coefficients $S_T = D_T/D$, which are experimentally obtained from the stationary amplitude of the concentration signal, are plotted in Fig. 3. The parametrizing solid lines are obtained from Eqs. (1) and (4) as

$$S_T = \frac{D_T}{D} = \frac{D_T^0}{a_0}\left(\frac{T - T_{sp}}{T}\right)^{-1}. \tag{10}$$

Compared to the critical scaling in the vicinity of the spinodal, thermal activation only weakly contributes to the temperature dependence of D and completely cancels out for S_T. Since the absolute variation of T is only moderate, the main contribution to the temperature dependence in Eqs. (1) and (10) arises from the term $T - T_{sp}$. Because the prefactors a_0 and D_T^0 are also almost concentration independent, both D and S_T fall on master curves when plotted as a function of ϵ, as shown in Fig. 1.

The phase diagram with the binodal, as obtained from turbidity measurements, and the approximate spinodal from the fit of Eq. (4) are plotted in Fig. 4. The lines are polynomial fits to the data points. The fit to the spinodal

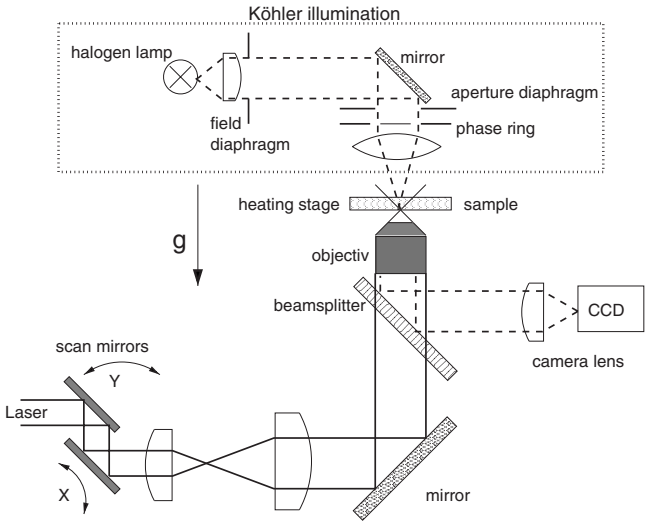

FIG. 5. Principle of experimental setup with schematic sketch of light paths of laser (solid line) and halogen lamp (dashed line).

$$T_{sp} = (-423.0c^4 + 356.8c + 200.3)\ \mathrm{K} \tag{11}$$

provides $T_{sp}(c)$ for the parametrization of D and S_T according to Eqs. (4) and (10), respectively. Similar phase diagrams have been reported for PDMS/PEMS of different molar masses by Alig *et al.* [14,28]. The color coding shows the Soret coefficient, which diverges at the spinodal but, except for the critical composition, remains finite at the phase boundary.

III. PATTERN WRITING

Especially the large Soret coefficients near a critical point can be utilized to write almost arbitrary composition patterns into a layer of the polymer blend by localized heating [6,10]. To demonstrate this, we have employed a phase contrast microscope setup in combination with a focused laser and a galvano scanner.

A. Setup

A sketch of the setup is shown in Fig. 5. It consists of an inverted phase contrast microscope with a laser port. Two mirrors mounted on magnet closed loop galvano scanners are situated in a conjugate (confocal) plane with a scanning point in the sample. The conjugate planes are formed with the help of two lenses (telecentric system) and an objective. The lenses expand the beam to ensure a complete illumination of the back focal plane of the objective. Objectives suitable for phase contrast and bright-field microscopy with various magnifications were applied for focusing a laser beam ($\lambda = 515$ nm) onto the sample. The laser focus in the middle of the cell is typically $r_0 = 0.8$ μm and its power can be tuned from 0.1 up to 100 mW.

The cell is mounted horizontally in a temperature-controlled xyz stage and hosts a polymer layer of thickness $L_s = 100$ μm, confined between two sapphire plates of thickness $L_w = 1$ mm. The sapphire cells are self-built, using a glass fiber as spacer and a two component epoxy (Torr Seal)

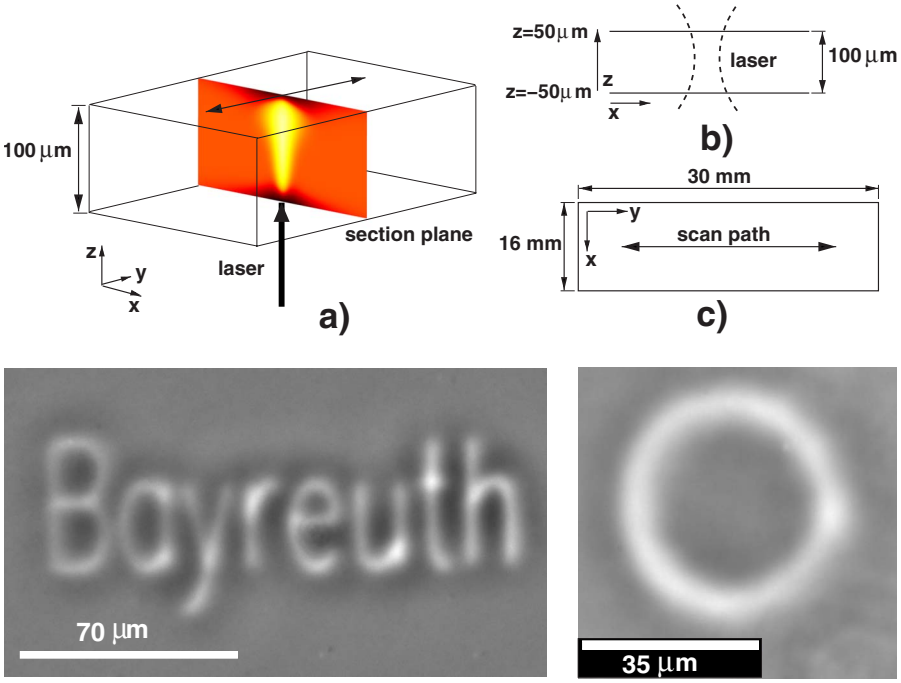

FIG. 6. (Color online) (a) Three-dimensional model of the cell. The laser beam propagates along the z axis and is scanned along the y axis. The two-dimensional simulation is carried out in the (x-z) plane as indicated by the section plane and sketch (b). Micrographs (Fig. 7) in the experiment are taken in the (x-y) plane as shown in (c). In (a) the spatial variation of the concentration in the (x-z) plane is color coded [see also Fig. 9(d)]. The word *Bayreuth* and the circle have been written by repeatedly scanning the laser across the surface.

to seal the two glass plates. The lateral dimensions of the cell are 30×16 mm (Fig. 6). A halogen lamp is used as a white light source and illuminates the sample with a Köhler illumination [29,30]. The same objective used for focusing the laser beam then maps the sample onto a CCD camera. Placing a phase ring in the back focal plane of the condenser lens turns this bright-field microscope into a phase contrast microscope. For taking a micrograph, a shutter in front of the laser is closed for 500 ms to avoid laser and fluorescence light in the observed image. The setup allows us to write arbitrary patterns in the xy plane of the sample with repeat frequencies up to 30 Hz on a micron scale. This is demonstrated in Fig. 6, where the word *Bayreuth* has been written as a composition pattern into the polymer slab.

B. Results

For the patterning experiments an almost symmetric PDMS(16.4 kg/mol)/PEMS(15.9 kg/mol) blend with a critical composition $c=c_{\mathrm{crit}}=0.48$ g/g and a convenient critical temperature $T_c=290.15$ K has been chosen. Some dye was added as described previously. Figure 1 shows D and S_T of this system.

Micrographs of the time evolution of the pattern at two different temperatures ($\Delta T=1$ K and $\Delta T=11.5$ K) above T_c are shown in Fig. 7. Until 100 s there is hardly a difference in the amplitudes of the concentration modulations, indicating an almost constant thermal diffusion coefficient D_T, which governs the early stage of the formation of the concentration pattern. At such short times, back diffusion as a competing process is still irrelevant. After 300 s this is no longer the case for the higher temperature. The growth of the structure becomes progressively limited by Fickian diffusion and solutal convection of the polymer, which aims at restoring the homogeneous state and, eventually, the Soret coefficient $S_T=D_T/D$ determines the maximum modulation depth. Close to T_c the structure is still within the initial linear growth regime after 300 s. After 2000 s the line for $\Delta T=1$ K becomes even more intense, whereas the line for $\Delta T=11.5$ K remains almost unchanged.

Due to the positive phase contrast technique, dark regions in the picture represent a higher refractive index compared to the bright regions. On the edge of the bright line a dark fringe can be seen, meaning that PEMS ($n=1.428$ at $T=20\,^{\circ}$C) migrates to the cold side, whereas PDMS ($n=1.404$ at $T=20\,^{\circ}$C) accumulates in the heated central region of the line. It should be pointed out, that the dark fringe around the line results not only from the accumulation of PEMS, but also due to a Halo effect in the applied phase contrast technique. We will discuss this point in more detail later. For now, we can state that the general behavior is in agreement with the measured sign of the Soret coefficient.

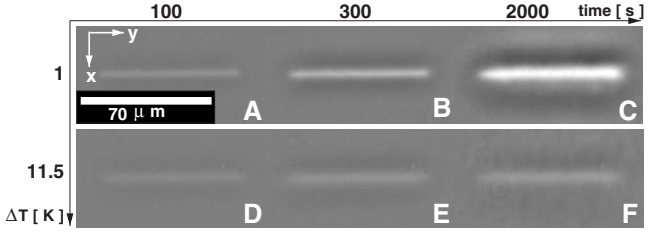

FIG. 7. Spatial modulation of concentration by scanning a laser along the y axis with a scanning frequency of 20 Hz and a laser power of 1 mW at two different temperatures above the critical temperature (see also Fig. 6). Pictures (A)–(C) taken at $\Delta T=1$ K after $t=100$ s, $t=300$ s, and $t=2000$ s. Pictures (D)–(F) taken at the same time intervals but at $\Delta T=11.5$ K. The intensity is normalized to the one of the undisturbed sample (picture at $t=0$ s). To display positive and negative changes, 127 is added to the 8-bit gray values. Gray values greater than 127 represent an increase of intensity, values smaller than 127 represent a decrease.

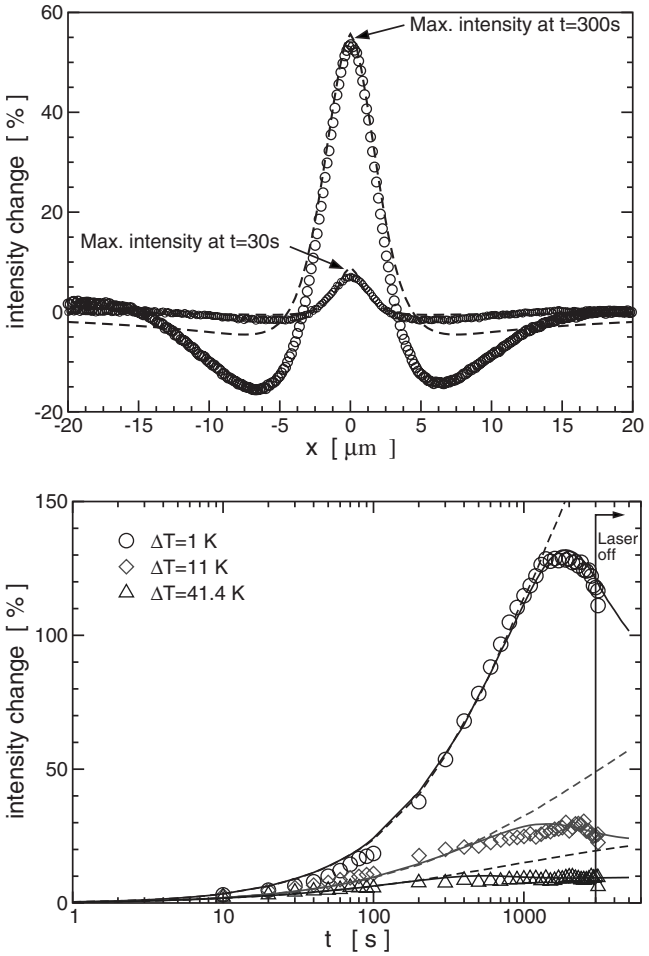

FIG. 8. (a) Intensity profile along the x axis, averaged over the length of the written line, taken from images (Fig. 7) at $t=300$ s and $t=30$ s for $\Delta T=1$ K. The open symbols show the result from the experimental pictures. The dashed lines show the numerical simulation (for details see Sec. IV). An increase of intensity (positive values) represents accumulation of PDMS. Far away from the written line the sample remains unchanged and the measured change of intensity equals zero. (b) Maximum intensity change obtained from averaged images plotted versus time at a laser power of 1 mW (open symbols) for different temperatures ΔT above the critical temperature. The vertical solid line indicates the switch-off time of the laser. The solid lines show numerical simulations with convection; the dashed lines show numerical simulations without convection.

Two intensity profiles along the x axis, averaged over the length of the written line, at $t=30$ s and $t=300$ s are shown in Fig. 8(a). With time proceeding, the profile becomes more pronounced. The intensity in the center ($x=0$ μm) grows by a factor of 5, but the linewidth (FWHM) remains at $\Delta x \approx 8$ μm. The intensity at the line fringe decreases with ongoing time. For distances from the center larger than ± 15 μm the intensity does not change at all, which means that the sample stays at the initial concentration far away from the heated region.

A plot of the maximum intensity change at different temperatures as a function of time is shown in Fig. 8(b). The intensity grows with time and reaches a maximum. As expected from the behavior of the Soret coefficient S_T, approaching the critical temperature increases the maximum achievable modulation depth. Due to the critical slowing down of the diffusion coefficient D, the time required for reaching the maximum modulation depth increases approaching T_c. The writing laser was switched off at a certain time as indicated in Fig. 8(b). Then, the profile slowly decays by Fickian diffusion. For clarity we only show the first points after the switchoff.

The phase contrast images provide sufficient information to identify PDMS as the component that enriches within the regions heated by the laser. Since the refractive index is integrated approximately along the optical path—the z direction in Fig. 6—no information about the true three-dimensional structure can be obtained. As heat not only diffuses horizontally within the image plane but also along the z direction into the sapphire windows, a complex three-dimensional structure develops. We will see below that a rather localized PDMS-rich channel develops along the line described by the laser focus. This channel is laterally confined by a polymer blend of average composition, and it is also shielded from the windows by a PEMS-rich layer.

IV. SIMULATIONS

In order to obtain a detailed picture of the three-dimensional structure we resort to numerical modeling. As input for the model the transport coefficients are needed as a function of both temperature and composition. Figure 1 clearly demonstrates that diffusion and Soret coefficients of different PDMS/PEMS blends are almost identical when plotted over ϵ for the respective critical compositions. This allows us to use the parametrizations of D and D_T determined for the PDMS(16.4 kg/mol)/PEMS(48.1 kg/mol) blend for the simulation of the patterning experiments on the PDMS(16.4 kg/mol)/PEMS(15.9 kg/mol). We determine T_c and c_c from the parametrized values and consider only temperature differences $\Delta T=T-T_c$ to simulate the behavior of the critical PDMS/PEMS sample used for thermal patterning.

A. Governing equations

Let us choose the Cartesian coordinates with the origin placed in the middle of the polymer layer and the z axis perpendicular to the confining plates [$z=\pm L_s/2$ for the upper (lower) plate] as shown in Fig. 6. The local heating of the sample is performed by the laser beam along the z axis moving back and forth parallel to the y axis. A typical length of a written line is about $L_{line} \approx 70$ μm, the incident laser power P_0 is 1 mW, and the scanning frequency is about $f=20$ Hz. The description of an incompressible binary mixture in the one-phase regime under inhomogeneous temperature field produced by light absorption is based on the heat equation for the temperature $T(\mathbf{r},t)$ and the diffusion equation for the concentration $c(\mathbf{r},t)$. The Navier-Stokes equation for the velocity $\mathbf{v}(\mathbf{r},t)$ is included to account for convection due to local heating. Thus, we start with the following set of equations.

The evolution of the temperature profile $T(\mathbf{r},t)$ is described by the heat equation

$$\partial_t T + (\mathbf{v}\cdot\boldsymbol{\nabla})T = \boldsymbol{\nabla}\cdot[D_{th}\boldsymbol{\nabla}T] + \frac{\alpha}{\rho c_p} I, \tag{12}$$

where D_{th} is the thermal diffusivity. The heat source term is proportional to the light intensity I that corresponds to the local illumination of the polymer film, α is the optical absorption coefficient, ρ is the mass density, and c_p is the specific heat at constant pressure. The intensity of the heating Gaussian laser beam that enters the polymer layer at $z=-L_s/2$ is given by

$$I = \frac{P_0}{A}\exp\left[-\frac{2\{x^2+(y-s)^2\}}{r^2}\right]\exp\left[-\alpha\left(\frac{L_s}{2}+z\right)\right],$$

$$A = \pi r^2/2, \quad r^2 = r_0^2\left[1+\left(\frac{\lambda z}{\pi r_0^2}\right)^2\right], \tag{13}$$

where $\lambda=515$ nm is the laser wavelength, and $s=s(t)$ describes the periodic scanning of the laser beam; in the experiments $s(t)$ changes from $-L_{line}/2$ to $L_{line}/2$ linearly in time.

The time evolution of the concentration profile $c(\mathbf{r},t)$ (weight fractions of PDMS) is governed by the diffusion equation

$$\partial_t c + (\mathbf{v}\cdot\boldsymbol{\nabla})c = \boldsymbol{\nabla}\cdot[D\boldsymbol{\nabla}c + D_T c(1-c)\boldsymbol{\nabla}T], \tag{14}$$

where D and D_T are the mass and the thermal diffusion coefficient, respectively.

Finally, one has the Navier-Stokes equation in the Boussinesq approximation

$$\rho_0[\partial_t\mathbf{v} + (\mathbf{v}\cdot\boldsymbol{\nabla})\mathbf{v}] = -\boldsymbol{\nabla}p + \eta_0\nabla^2\mathbf{v} - \rho g\mathbf{e}_z, \tag{15}$$

and incompressibility condition

$$\boldsymbol{\nabla}\cdot\mathbf{v} = 0. \tag{16}$$

In Eq. (15) the density of the mixture ρ depends on the temperature only in the buoyant term

$$\rho = \rho_0[1-\beta_T(T-T_0)+\beta_c(c-c_0)]. \tag{17}$$

ρ_0 is the mean density at temperature T_0 (ambient temperature), $\beta_T=-(1/\rho)(\partial\rho/\partial T)_c$ is the thermal expansion coefficient, and $\beta_c=(1/\rho)(\partial\rho/\partial c)_T$ is the solutal expansion coefficient.

B. Two-dimensional model

To describe the temperature and concentration distributions in the cross section of the polymer layer (x-z plane) located in the middle of the written line, we consider a two-dimensional model supposing the line to be infinitely extended in the y direction. Consequently, T, c, and $\mathbf{v}$ are independent on y. This is a good approximation if the length of the line is larger than the temperature decay length from the written line along the x axis. Under experimental conditions the temperature decay length is about 25–50 μm. The intensity of the heating laser beam is given by averaging over the scan period of Eq. (13) taken at $y=0$,

$$I = (P_0/A)\exp\left[-\frac{2x^2}{r^2}\right]\exp\left[-\alpha\left(\frac{L_s}{2}+z\right)\right],$$

$$A = \sqrt{\frac{\pi}{2}}\frac{rL_{line}}{\mathrm{erf}(L_{line}/\sqrt{2}r)},$$

$$r^2 = r_0^2\left[1+\left(\frac{\lambda z}{\pi r_0^2}\right)^2\right]. \tag{18}$$

Since the thermal conductivity of the sapphire plates [$\kappa_s=42$ W/(m K)] confining the polymer layer is about 250 times larger than the one of PDMS/PEMS, we use the approximation of perfectly conducting plates with fixed temperature boundary conditions

$$T = T_0 \tag{19}$$

for the polymer layer at the boundaries of the rectangular region $z=\pm L_s/2$ and $x=\pm L_x/2$. In order to avoid the influence of lateral boundaries we choose in our simulations the width of the layer $L_x=400$ μm, which allows us to monitor the concentration dynamics for time $t\leqslant 10^4$ s.

The boundary conditions for the diffusion equation (14) correspond to zero mass flux

$$\boldsymbol{\nu}\cdot[D\boldsymbol{\nabla}c + D_T c(1-c)\boldsymbol{\nabla}T] = 0, \tag{20}$$

where $\boldsymbol{\nu}$ is a normal to the boundary. For the velocity one has no slip boundary conditions $\mathbf{v}=0$ at $z=\pm L_s/2$ and $x=\pm L_x/2$. Initial conditions at $t=0$ are $T=T_0$, $c=c_0$, and $\mathbf{v}=0$. Numerical simulations of Eqs. (12)–(16) in 2D have been performed using finite differences with an adaptive mesh refinement technique.

To compare the results of simulations with experimental phase contrast microscopy measurements we adopt the expression for transmitted light intensity in the ideal positive phase contrast imaging [29,30]

$$I_{Tr} = 1 + p^2 + t^2 - 2p(\cos\phi + t\sin\phi),$$

$$\phi = \frac{2\pi L_s}{\lambda_{hal}}\frac{\partial n}{\partial c}(\bar{c}-c_0), \tag{21}$$

where $p^2=1$ is the relative amplitude transmittance of the polymer layer, $t^2=0.4$ is the relative transmittance of the microscope objective, $\phi=\phi(x)$ is the phase shift induced in the layer due to the concentration change, $\lambda_{hal}=550$ nm is the wavelength of probing light, $\partial n/\partial c=-2.3\times10^{-2}$ is the contrast factor of the PDMS/PEMS mixture, and $\bar{c}$ is the concentration averaged over the layer thickness.

Expression (21) is obtained under the assumption that the phase object width (in the plane perpendicular to the light propagation direction) is much larger than the phase object thickness. In our case the width of the region with strong concentration change is about 10–20 μm, whereas the thickness of the layer is 100 μm. This does not allow one to use Eq. (21) directly for quantitative calculations. An analysis of the quantitative phase contrast microscopy [31] shows that decreasing of the phase object width effectively leads to the reduction of the actual phase shift and consequently reduces

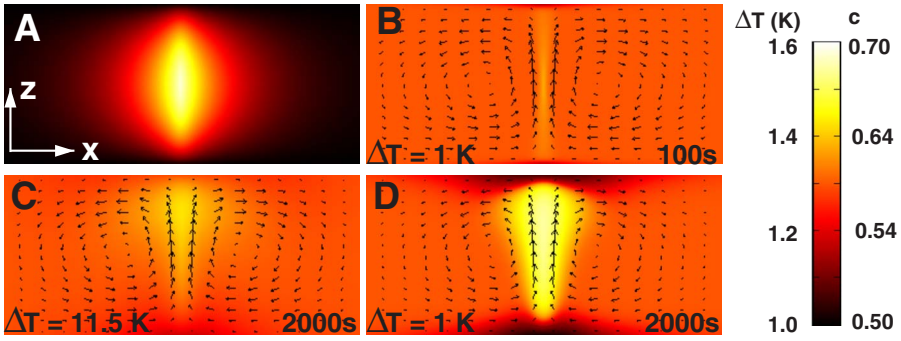

FIG. 9. (Color online) Temperature profile (A), concentration profile at $t=100$ s (B), and concentration profile at $t=2000$ s for $\Delta T=1$ K (D) and $\Delta T=11.5$ K (C). Sample thickness (z axis) 100 μm.

the measured intensity compared to the one obtained from Eq. (21). Thus, the relative change of the intensity can be written as

$$\frac{I_{Tr}-I_{Tr0}}{I_{Tr0}}=K\left[\frac{1+p^2+t^2-2p(\cos\phi+t\sin\phi)}{1+p^2+t^2-2p}-1\right], \tag{22}$$

where $K\leqslant 1$ is the parameter which depends on the ratio of the width and thickness of the phase object. Since in our case the sizes of the region with high concentration change are nearly the same for different temperatures T_0 we will use K as a "fitting" parameter when comparing the results obtained from Eq. (22) with experimental data.

C. Material parameters

Since PDMS and PEMS have comparable densities ρ, specific heats c_p and thermal diffusivities $D_{th}=\kappa/(\rho c_p)$ m^2/s, we have used the following material parameters of PDMS at room temperature in the heat equation (12) [32]: thermal conductivity $\kappa=0.16$ W/(mK), specific heat at constant pressure $c_p=1.6\times10^3$ J/(kg K), and a measured optical absorption coefficient $\alpha=5$ cm^{-1}. In addition, the temperature variation due to local heating is small (does not exceed 1 K for $P_0=1$ mW) therefore we can consider the parameters c_p and κ to be constant when studying the temperature distribution within the polymer film. The critical concentration $c_c=0.596$ and temperature $T_c=359.6$ K for the simulations are obtained from Eq. (11). In the diffusion equation (14) we have used for the mass diffusion coefficient $D=D(T,c)$ [Eq. (4)] with T_{sp} from Eq. (11). D_T is given by Eq. (2). In the Navier-Stokes equation (15) we have used for the mean viscosity η_0 at the mean sample temperature T_0 [33],

$$\eta_0=2.5\exp\left(-\frac{T_A}{T_0}\right)\times10^{-3}\ [\text{Pa s}]. \tag{23}$$

The thermal and solutal expansion coefficients have been calculated using the expression for the mass density of mixture

$$\rho=\left(\frac{c}{\rho_{\text{PDMS}}}+\frac{1-c}{\rho_{\text{PEMS}}}\right)^{-1}, \tag{24}$$

with [34]

$$\rho_{\text{PDMS}}=[0.990-7.3\times10^{-4}(T/\text{K}-273)]\ \text{g/cm}^3, \tag{25}$$

$$\rho_{\text{PEMS}}=[0.986-5.4\times10^{-4}(T/\text{K}-273)]\ \text{g/cm}^3. \tag{26}$$

Let us now estimate the separation ratio for a PDMS/PEMS mixture $\psi=D_T\beta_c/(D\beta_T)$ at $T=T_0$, $c=c_c$ at three different temperatures above the critical temperature T_c as follows:

$$T_0=T_c+1\ \text{K}:\psi=499.5,$$

$$T_0=T_c+11\ \text{K}:\psi=55.6,$$

$$T_0=T_c+41.4\ \text{K}:\psi=22.3.$$

The above separation values are calculated with a constant Soret coefficient, corresponding to the critical concentration. Because of the strong concentration dependence of S_T, the actual concentration changes are smaller than estimated from equilibrium. Our simulations show that for $T-T_0<10$ K the density change caused by the Soret effect exceeds the one caused by the pure thermal expansion. For the fully developed convection the amplitude of the velocity can be roughly estimated from above supposing that at $x=0$ the velocity has only a z component $v_z\approx v_0[1-(2z/L_s)^2)]$,

$$v_0\approx\frac{\rho_0 g L_s^2}{8\eta_0}[\beta_T(T-T_0)-\beta_c(c-c_0)]. \tag{27}$$

D. Results

The results of the simulations are shown in Fig. 9. The temperature profile induced by the laser is shown in Fig. 9(a). Because of an almost constant D_T, the resulting concentration profile is almost independent of the overall sample temperature for short times ($t<100$ s). The surprisingly narrow and sharp concentration profile induced by the broad temperature profile results from the fact that at the initial stage only $\nabla^2T\propto I$ drives the concentration change, and not T.

Figure 9 also shows the concentration profile for $\Delta T=11.5$ K [picture (C)] and $\Delta T=1$ K [picture (D)] at $t=2000$ s. For $\Delta T=1$ K the concentration modulation is more pronounced than for $\Delta T=11.5$ K. Both profiles lost their symmetry due to solutal convection. In the long time regime this Soret driven convection limits the maximum achievable concentration shifts. It should be noted that for the investigated PDMS/PEMS system solutal expansion plays the dominant role for convection. As tested by numerical simulations, the effect of radiation pressure of the absorbed light

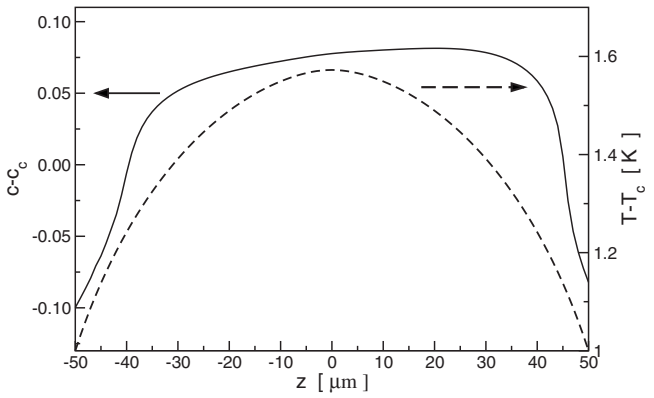

FIG. 10. Temperature profile (dashed line) and concentration profile (solid line) along the z axis for $\Delta T=1$ K and $t=2000$ s. The left axis shows the concentration change and the right axis belongs to the temperature profile.

is approximately one order of magnitude smaller and, hence, negligible.

Due to the constant temperature at the cell windows, the temperature gradient towards them is significant. The simulations show that the maximum temperature gradient along the x axis, which is close to the middle point in the cell, is smaller than the gradient along the z axis at the cell windows. This causes a strong decrease of PDMS at the cell windows. The concentration and temperature profile is plotted along the z axis in Fig. 10 for $\Delta T=1$ K, a maximum temperature rise of 0.6 K and a maximum concentration difference $c-c_0\approx 0.1$ is found.

To visualize what region the sample occupies in the phase diagram, the temperature rise and concentration change are plotted in Fig. 11 for every point along the z axis. At the cell windows ($z=\pm 50$ μm) only the concentration changes,

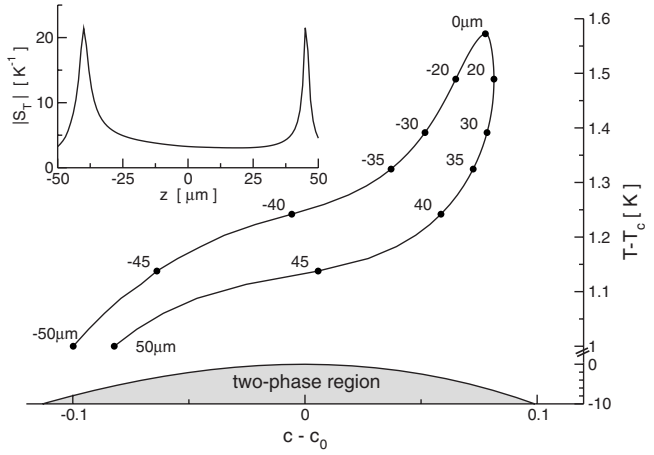

FIG. 11. Concentration change and temperature change plotted for each point on the z axis at $t=2000$ s. In the center of the sample ($z=0$) the temperature increases and the composition changes to a higher concentration of PDMS. At $z=\pm 50$ μm the cell is held at constant temperature $\Delta T=1$ K above T_c; only the concentration shifts. The maximum concentration change is found at the lower cell window $z=-50$ μm. The plot shows what complex area the sample occupies in the phase diagram during thermal patterning. The inset shows how the Soret coefficient varies along the z axis.

whereas in the center of the sample ($z=0$ μm) both the temperature increases and the concentration changes. At the bottom of the graph the parametrized experimental spinodal is plotted and the inset shows the local Soret coefficient along the z axis. The laser heating and the following concentration shift always leads to a local decrease of the Soret coefficient and also limits the achievable concentration modulations.

To compare the experimental results with the simulations we calculated the phase shift of light passing along the z axis. The phase shift is then, with Eq. (22), converted into an intensity change. This intensity value is compared to the maximum intensity change obtained from the micrographs. Figure 8(b) shows both, experimental and theoretical results. The scale factor K from Eq. (22) is chosen to $K=1/6.54$ for all curves. The simulation can reproduce the characteristic features of the experimental data. The plateau for long times results only from solutal convection, since calculations without convection show that no plateau can be reached within this time.

A comparison of not only the maximum intensity change, but also along the whole x axis is shown in the comparison of the averaged cross section in Fig. 8(a). The simulated intensity profiles agree with the experiments over the whole linewidth. For distances exceeding the linewidth the experiments show a stronger reduction of the intensity than the simulations. The reason lies in K, which depends on the geometry of the phase object the light is passing through. K is larger for objects with a larger aspect ratio (width/height), which holds for the wings when compared to the center of the structure. Thus, the concentration modulation, and therefore the phase object, away from the center is completely different and K had to be chosen differently to find agreement there. Additionally, Eq. (22) does not include Halo effects in phase contrast microscopy and especially towards the edge of the line Halo effects become more important.

V. SUMMARY AND CONCLUSIONS

We have shown that almost arbitrary composition patterns can be written into a thin layer of a polymer blend by means of a focused laser beam. The underlying mechanism is thermal diffusion, which becomes especially effective near the critical point, where the Soret coefficient diverges. As heat flows away from the heated regions, both temperature and concentration and, as a consequence, also the transport coefficients become rather complex space and time dependent fields. This is best seen in Fig. 11, where the excursion in the phase diagram and the corresponding variation of the Soret coefficient is plotted for a cross section through the sample. We have been able to obtain a quantitative description from a numerical model which is based on the heat and the diffusion equation with additional terms to include thermal diffusion. An additional advection term, obtained from the Navier-Stokes equation in the Boussinesq approximation, results mainly from solutal convection caused by the concentration changes. Besides trivial quantities such as density, the transport coefficients both as a function of temperature and concentration were needed for the numerical analysis. Neither the thermal diffusion nor the Soret coefficient were known

for any polymer blend. As they also cannot reliably be predicted from other material properties, we performed extensive transient holographic grating experiments to measure these coefficients. For the parametrization of the data we resorted to the pseudospinodal concept. Since different molar masses have been involved in the experiments, the temperatures have been shifted to match the critical temperatures, which has been validated by comparing the transport coefficients of different near-critical mixtures. Due to the complicated three-dimensional structures with different aspect ratios, an empirical factor had to be introduced for the quantitative interpretation of the phase contrast micrographs.

A detailed analysis of a cross section of the concentration profiles (Fig. 9) reveals that sharp structures defined by the width of the laser beam are formed in the early stage although the driving temperature field has already reached its broad stationary profile [Figs. 9(a) and 9(b)]. This follows as a direct consequence from the structure of the governing heat and diffusion equations.

Another unexpected property of these localized channels with PDMS enrichment is the formation of thin PEMS-rich layers that shield the channels from the window material. The color coding (hot-cold colormap) in Fig. 9(d) can directly be interpreted in terms of a refractive index map. Although the sign of the refractive index change in the PDMS/PEMS system is such that the channel has a lower refractive index, one can envisage the opposite case, where the channel can be viewed as a gradient index waveguide with additional cladding layers [dark in Fig. 9(d)] of lower refractive index that isolate the waveguide from the high refractive index substrate. In such a material the written arbitrary lines could serve as reconfigurable optical waveguides. Other possible applications could be optically adjustable and tunable optical phase plates, such as Fresnel zone plates [35]. Written structures are fully reversible and can be erased by heating. Long term stability could be obtained with blends consisting of a polymer with a low and one with a high glass transition temperature, where the dynamics comes to arrest during demixing [23].

ACKNOWLEDGMENTS

We thank G. Meier and I. Alig for helpful discussions and T. Wagner for providing samples. This work was supported by the Deutsche Forschungsgemeinschaft (SFB481/A8).

[1] H. Nakayama, O. Sugihara, and N. Okamoto, Appl. Phys. Lett. **71**, 1924 (2006).
[2] M. Böltau, S. Walheim, J. Mlynek, G. Krausch, and U. Steiner, Nature (London) **391**, 877 (1998).
[3] H. J. Chung, H. Wang, and R. J. Composto, Macromolecules **39**, 153 (2006).
[4] B. Loppinet, E. Somma, N. Vainos, and G. Fytas, J. Am. Chem. Soc. **127**, 9678 (2005).
[5] R. Sigel, G. Fytas, N. Vainos, S. Pispas, and N. Hadjichristidis, Science **297**, 66 (2002).
[6] A. Voit, A. Krekhov, W. Enge, L. Kramer, and W. Köhler, Phys. Rev. Lett. **94**, 214501 (2005).
[7] W. Enge and W. Köhler, Phys. Chem. Chem. Phys. **6**, 2373 (2004).
[8] J. Luettmer-Strathmann, in *Thermal Nonequilibrium Phenomena in Fluid Mixtures*, edited by W. Köhler and S. Wiegand (Springer, Heidelberg, 2002), p. 24.
[9] S. Duhr and D. Braun, Proc. Natl. Acad. Sci. U.S.A. **103**, 19678 (2006).
[10] A. Voit, A. Krekhov, and W. Köhler, Macromolecules **40**, 9 (2007).
[11] D. B. Wolfe, R. S. Conroy, P. Garstecki, B. T. Mayers, M. A. Fischbach, K. E. Paul, M. Prentiss, and G. M. Whitesides, Proc. Natl. Acad. Sci. U.S.A. **101**, 12434 (2004).
[12] S. Sakurai,Y. Wang, T. Kushiro, T. Nambu, and S. Nomura, Chem. Phys. Lett. **348**, 242 (2001).
[13] G. Meier, B. Momper, and E. W. Fischer, J. Chem. Phys. **97**, 5884 (1992).
[14] I. Alig, M. Rüllmann, M. Holst, and J. Xu, Macromol. Symp. **198**, 245 (2003).
[15] W. Enge and W. Köhler, Eur. Phys. J. E **15**, 265 (2004).
[16] G. Wittko and W. Köhler, Philos. Mag. **83**, 1973 (2003).
[17] J. M. O. de Zarate, R. P. Cordon, and J. V. Sengers, Physica A **291**, 113 (2001).
[18] B. Chu, F. J. Schoenes, and M. E. Fisher, Phys. Rev. **185**, 219 (1969).
[19] S. Eckert, S. Hoffmann, G. Meier, and I. Alig, Phys. Chem. Chem. Phys. **4**, 2594 (2002).
[20] M. Hartung, J. Rauch, and W. Köhler, J. Chem. Phys. **125**, 214904 (2006).
[21] J. Rauch and W. Köhler, J. Chem. Phys. **119**, 11977 (2003).
[22] W. Theobald and G. Meier, Phys. Rev. E **51**, 5776 (1995).
[23] G. Meier, D. Vlassopoulos, and G. Fytas, Europhys. Lett. **30**, 325 (1995).
[24] G. Meier, G. Fytas, B. Momper, and G. Fleischer, Macromolecules **26**, 5310 (1993).
[25] B. Momper, G. Meier, and E. W. Fischer, J. Non-Cryst. Solids **131**, 624 (1991).
[26] K. Binder, Adv. Polym. Sci. **112**, 181 (1994).
[27] G. Strobl, *The Physics of Polymers* (Springer, Berlin, 1996).
[28] M. Rüllmann and I. Alig, J. Chem. Phys. **120**, 7801 (2004).
[29] R. Beyer, *Handbuch der Mikroskopie*, 2nd ed. (VEB Verlag Technik, Berlin, 1977).
[30] M. Born and E. Wolf, *Principles of Optics* (Cambridge University Press, New York, 1998).
[31] C. J. Bellair, C. L. Curl, B. E. Allman, P. J. Harris, A. Roberts, L. M. D. Delbridge, and K. A. Nugent, J. Microsc. **214**, 62 (2004).
[32] D. van Krevelen, *Properties of Polymers*, 3rd ed. (Elsevier, Amsterdam, 1990).
[33] W. Enge, Ph.D. thesis, University Bayreuth, 2004 (unpublished).
[34] S. Enders, A. Stammer, and B. Wolf, Macromol. Chem. Phys. **197**, 2961 (1996).
[35] H. Ren, Y. Fan, and S. Wu, Appl. Phys. Lett. **83**, 1515 (2003).